Quasi-Solid-State Electrochromic Cells with Energy Storage Properties Made with Inkjet Printing

Krystallia Theodosiou [1], **Panagiotis Giannopoulos** [1], **Tilemachos Georgakopoulos** [1] and **Elias Stathatos** [1,2,*]

[1] BRITE Solar Technologies, Patras Science Park, Stadiou Str., Platani, 26504 Patras, Greece; ktheodosiou@britesolar.com (K.T.); pgiannopoulos@britesolar.com (P.G.); tgeorga@britesolar.com (T.G.)

[2] Nanotechnology and Advanced Materials Laboratory (NAML), Electrical and Computer Engineering, University of the Peloponnese, 26334 Patras, Greece

[*] Correspondence: estathatos@uop.gr; Tel.: +30-2610-369242

check for updates

Abstract: In common commercially available electrochromic glass panes, the active materials such as WO_3 and NiO_x films are typically deposited by either physical vapor or sputtering under vacuum. In the present studies, we report on the inkjet printing method to deposit both electrochromic and ion storage electrode layers under ambient conditions. An ion storage layer based on cerium modified TiO_2 and electrochromic nanocrystalline WO_3 were both prepared under the wet method and deposited as inks on conductive substrates. Both compounds possess porous morphology facilitating high ion diffusion during electrochemical processes. In particular, the ion storage layer was evaluated in terms of porosity, charge capacity and ion diffusion coefficient. A scaled up 90 cm^2 electrochromic device with quasi-solid-state electrolyte was made with the aforementioned materials and evaluated in terms of optical modulation in the visible region, cyclic voltammetry and color efficiency. High contrast between 13.2% and 71.6% for tinted and bleached states measured at 550 nm was monitored under low bias at +2.5 volt and −0.3 volts respectively. Moreover, the calculated energy density equal to 1.95×10^{-3} mWh cm^{-2} and the high areal capacitance of 156.19 mF cm^{-2} of the device could combine the electrochromic behavior of the cell with energy storage capability so as to be a promising candidate for future applications into smart buildings.

Keywords: electrochromic cells; energy storage; cerium-modified Titanium dioxide; quasi-solid-state electrolyte

1. Introduction

The high need for green technology and reduced energy consumption over the last decades has led to the development of various chromogenic materials. Chromogenic materials have the ability to change their optical properties as a response to an external stimulus. Typical examples are photochromic, thermochromic and electrochromic materials [1–3]. The materials that are able to change their optical properties, when an electric potential is applied are called electrochromic (EC) and probably have been most studied among the rest of the chromogenic materials. This optical change is reversible after suitable bias and is accompanied by injection and extraction of electrons and small ions (such as H^+ and Li^+) [4,5]. An ideal EC device would provide high optical contrast, fast switching time between colored and clear states, long cycle life and low manufacturing cost [6]. Due to the high need for significant energy saving, the current electrochromic research is aiming to develop electrochromic windows, usually called "smart" windows. A smart window is applicable across all building types and can be used in order to achieve improved energy efficiency, through the control of the transmittance of sunlight and solar heat into a building [7–9].

A typical EC device consists of five layers, as presented in Figure 1: two transparent conducting layers (typically conductive glass substrates, SnO_2:F (FTO)), the EC layer, an ion storage layer and an ion conductor among them, typically referred to as electrolyte in liquid systems [10]. The EC layer may consist of a "cathodic" EC material (materials that can be colored under cation insertion), or an "anodic" EC material (coloration under anion insertion). However, an EC device could also participate with EC layers of both types, one of them consisting of cathodic EC material and the other consisting of anodic EC material. Both layers have to color simultaneously under a specific external bias voltage, in order to achieve the maximum device coloration. A great number of materials, such as organic molecules, conducting polymers and transition metals, have been used for the development of EC devices. Tungsten(VI) trioxide (WO_3) is the most widely studied electrochromic material. WO_3 can be colored under cation or proton insertion (cathodic EC material).
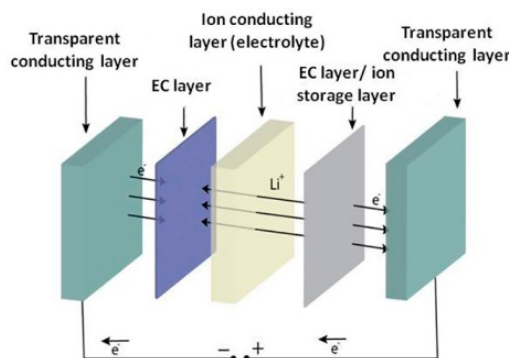

Figure 1. Typical structure of an electrochromic (EC) device.

Titanium dioxide (TiO_2), Niobium pentoxide (Nb_2O_5) and Molybdenum trioxide (MoO_3) have also been used as cathodic EC materials. The films based on the above materials have the ability to change their color from transparent or pale yellowish to blue or brown, due to electrochemical reduction. Among all electrochromic materials, WO_3 is considered to have the best overall performance, due to its high coloration efficiency, good cycling life and fast switching time. On the other hand, the majority of the rest of the widely studied cathodic EC materials have shown either low coloration efficiency, or poor durability over electrochemical cycling [6,11–14]. The electrochemical reduction that leads to the coloration of WO_3 can be written as:

$$\underset{\text{transparent}}{WO_3} + x\left(A^+ + e^-\right) \rightarrow A_x W^{VI}_{(1-x)} W^{V}_{x} \underset{\text{blue}}{O_3} \tag{1}$$
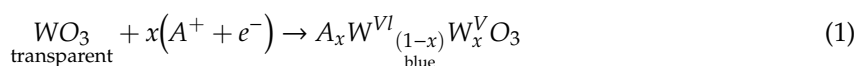
which A^+ refers to H^+, Li^+, Na^+;

Anodic EC materials can be colored by electrochemical oxidation and are usually employed as counter electrodes (CE). The most popular anodic EC material is nickel oxide (NiO), whereas iridium dioxide (IrO_2), vanadium pentoxide (V_2O_5), and organic-, metallo-organic or polymeric complexes have also been used [15–21]. The electrochemical reaction of NiO coloration in alkaline aqueous solution can be described as:

$$\underset{\text{transparent}}{NiO} + OH^- \rightarrow \underset{\text{brown}}{NiOOH} + e^- \tag{2}$$
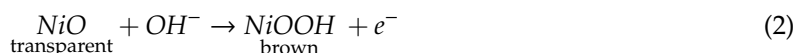
In a different approach, when a second EC material is not used as it is difficult to achieve a simultaneous operation of both electrochromic materials by the same electrolyte, an optically passive layer can be used as the counter electrode. Films based on cerium dioxide (CeO_2), tin dioxide (SnO_2) or zirconium dioxide (ZrO_2) have been widely used [22–25]. In this approach, the coloration of the EC device is due to the coloration of only one EC layer. The optically passive layer acts as an ion-storage layer and presents high and stable optical transmittance in both oxidized and reduced states. In a slightly modified approach, one electrode can act simultaneously as electrochromic and energy-storage layer [26].

There are several methods that have been tested for the preparation of EC layers or ion-storage layers [27,28]. Most of them are solution-based, such as spray pyrolysis [29,30], the sol-gel method [31,32] and electrodeposition [33,34]. Among these, the sol-gel process is low-cost and can be easily used for the preparation of large area films, through various techniques. One of the most promising techniques, employing sol-gel prepared solutions, is inkjet printing. The inkjet printing process has the advantage of precise, high speed and contact-less deposition in single- or multi-layer constructions at a very affordable price [35,36]. Additionally, through inkjet printing the material wastes are limited, the process is quite simple and applicable to a variety of substrates and high resolution can be achieved [37–39]. On the other hand, it is very important to control the ink properties (viscosity, surface tension and evaporation rate) and printing settings, in order to achieve a very homogenous film [40]. In consequence, even if a great number of works over recent years have focused on inkjet printing technology, there is no standard protocol for the preparation of suitable inks for inkjet printing and various obstacles have been observed (unstable inks, inhomogeneous films, nozzle clogging and so on) [41].

Finally, the selection of an appropriate ion conductor (electrolyte) is also a critical parameter for the electrochemical process. The electrolyte must be chemically stable under electrochemical cycling, with as fast a response time as possible. Common organic solvents are usually not used, due to their toxicity, flammability and high volatility [42,43]. Therefore, gel electrolytes based on polymers or ionic liquids (ILs) are much more desirable. Gel electrolytes have been used in various applications such as dye-sensitized solar cells, batteries and supercapacitors, whereas they present higher ionic conductivity than solid electrolytes [44–49].

In the present work, we report on the preparation of a quasi-solid-state EC device based on a WO_3 EC layer and an ion-storage layer based on cerium-modified TiO_2. The final solutions were prepared by a very simple procedure, without steps such as centrifugation, filtration or other techniques that usually are necessary. The above electrodes were prepared using the inkjet-printing method by suitable deposition of inks composed of the aforementioned materials on FTO glass, while their morphological and electrochemical properties have been investigated. The electrolyte used was based on a nanocomposite organic-inorganic gel, prepared using the sol-gel procedure. Through this route, the electrolyte provides good ionic conductivity and simultaneously works as a gluing material holding the two electrodes together. The above device presents excellent electrochemical stability and optical reversibility between clear and colored states, and has supercapacitance properties too. The specific approach is very promising and can be used in large-scale production for the preparation of smart windows. Our goal was the preparation of samples that can be easily produced and used in large scale applications, so great attention was paid to the detail, in order to achieve a fully homogeneous sample, free of even small irregularities that are usually observed in most research works.

2. Materials and Methods

2.1. Chemical Materials and Characterization Techniques

Commercial titanium (IV) isopropoxide (TTIP, 97%, Sigma-Aldrich, St. Louis, MO, USA), Triton X-100 (Sigma-Aldrich, St. Louis, MO, USA), glacial acetic acid (AcOH, 99–100%, Sigma-Aldrich, St. Louis, MO, USA), ethanol (absolute, 99.5% Sigma-Aldrich, St. Louis, MO, USA) and cerium(III) nitrate hexahydrate (90%, Sigma-Aldrich, St. Louis, MO, USA), were used to make Ce modified-TiO_2 precursor sols. Tungsten powder (99.9%, Sigma-Aldrich, St. Louis, MO, USA) and hydrogen peroxide solution (30% in water, Sigma-Aldrich, St. Louis, MO, USA) were used to prepare the WO_3 precursor sol. All solvents were purchased from Sigma-Aldrich and they were used as received. SnO_2:F transparent conductive electrodes (FTO, TEC[TM] A8) with 8 Ω/sq were purchased from Pilkington NSG Group (Tokyo, Japan).

O,O′-Bis(2-aminopropyl) polypropylene glycol-block-polyethylene glycol-block-polypropylene glycol (Jeffamine®ED-600, Mr~600) and 3-isocyanatopropyltriethoxysilane (ICS; molar ratio

ICS/diamine = 2) were used for the synthesis of hybrid organic/inorganic material abbreviated as ED-600-ICS which were put in a vessel to react (acylation reaction), producing urea connecting groups between the polymer units and the inorganic part. The as-prepared hybrid organic/inorganic material ED-600-ICS is necessary for the quasi-solid-state electrolyte according to the procedure described in our previous publications [50,51].

Electrochemical measurements were carried out in a three-electrode cell with the use of an Autolab PGSTAT 302N electrochemical analyzer (Metrohm AG, Herisau, Switzerland). All experiments were carried out in freshly prepared 1.0 mol L^{-1} $LiClO_4$ in PC as the electrolyte. The working electrode was either the WO_3 film or the cerium-modified TiO_2 film deposited on FTO coated glass, the reference electrode was Ag/AgCl and the counter electrode was a platinum foil. In particular, for the double-junction electrode Ag/AgCl, the reference electrolyte was LiCl 2mol/L in ethanol and the bridge electrolyte was $LiClO_4$ 1 mol/L in propylene carbonate (PC). The ultraviolet-visible/NIR absorption diffuse reflectance spectra of the electrochromic films and devices were obtained at ambient conditions in a range of 300 to 2500 nm using a Jasco V-770 spectrophotometer (Jasco, Easton, PA, USA) equipped with a 60 mm integrating sphere embedding a PbS detector (ISN-923). Nanostructure morphology of the films was studied by field-emission electron microscopy (FE-SEM, Zeiss SUPRA 35VP) and TEM microscopy, JEOL (JEM-2100, Yamaguchi, Tokyo). As the porosity of the ion storage layer in electrochromic cells is very important the stuctural properties of the Ce modified-TiO_2 were also evaluated with porosimetry. Nitrogen adsorption/desorption curves for these samples were measured with a Micromeritrics Tristat 3000 and the surface area and pore size distribution were derived by differentiating them according to the BET method. Finally, the inkjet printing technique was performed using the Fujifilm Dimatix printer (DMP2850); the printheads that were employed for film deposition of all materials consisted of sixteen nozzles depositing 10 pl drop volumes.

2.2. Development of Electrochromic Materials and Films

2.2.1. Tungsten Trioxide Thin Layers

The preparation of tungsten trioxide (WO_3) films was carried out by an inkjet printing technique on FTO glass substrates. The first step involved a highly exothermic reaction between 5 g of W powder and 20 mL of hygrogen peroxide (H_2O_2), which led to the formation of peroxotungsten acid (PTA) [33]. In the above solution, a mixture of Triton X-100 and 2-Propanol with an optimized molar ratio 1/70 = Triton X-100/2-Propanol was then added. The final ink contained 28 mmol of tungsten per 60 mL of sol. Triton X-100, a nonionic long chain surfactant, was selected as a pore directing agent in the solution. Compared to other commonly used toxic and ionic templating agents, Triton X-100 is relatively inexpensive, non-toxic, and easily removable. Such amphiphilic molecules exhibit ordered mesophase and the ability to adjust large inorganic clusters in aqueous condition [52,53]. The final tungsten ink had surface tension equal to 30 dynes/cm, viscosity equal to 11 cPs, density equal to 1.1 g/ml and was filtered through a 0.2 μm PTFE filter before being used in the printing procedure. Small and spherical drops were achieved, while a 20 μm drop spacing was employed. The reliability and repeatability of the film was excellent during printing. The film was deposited on SnO_2:F (FTO) coated glass 3.2 mm thick. Before deposition, the substrates were cleaned with soft detergent, rinsed with deionized water and calcined at 500 °C for 10 min in order to remove moisture and any organic residues. The as-prepared WO_3 films were uniform and optically transparent.

2.2.2. Cerium Modified-TiO_2 Thin Films as Ion Storage Layers

A suitable amount of Triton X-100 was homogeneously dissolved in ethanol (EtOH). Before adding titanium(IV) isopropoxide precursor (TTIP), AcOH was added into the solution. Then, the TiO_2 precursor TTIP was added during vigorous stirring. The molar ratio of the materials was optimized at Triton X-100:EtOH:AcOH:TTIP = 1:69:6:1. Cerium(III) nitrate was finally added to the previous solution in various quantities before we concluded determination of the optimal ratio. We finally

kept 10% weight ratio of cerium nitrate in the TTIP solution as the optimized concentration for our experiments because the electrochromic properties of our devices were also optimized. The final ink was printed using the same parameters as for the tungsten ink since the physical properties of the two inks were comparable. After several minutes, the dispersion was ready to be used on glass slides. Films prepared on FTO glass were also prepared with the inkjet printing process as in the case of WO_3. The as-prepared films were also uniform and optically transparent as in the case of WO_3.

2.2.3. Synthesis of Quasi-Solid-State Electrolyte and Completion of the EC Device

1.2 grams of sulfolane (>99.5%, Sigma-Aldrich, St. Louis, MO, USA) were mixed with 0.29 grams of ED-600-ICS organic-inorganic hybrid substance followed by an addition of 0.092 grams of acetic acid (>99.85%, Alfa Aesar, Haverell, MA, USA), and finally of 0.082 grams of anhydrous $LiClO_4$ (>99.5%, Sigma-Aldrich, St. Louis, MO, USA). The quasi-solid-state electrolyte was prepared just before the completion of the EC assembly to avoid any gelation process to start before finalizing the device. After preparing the aforementioned films by inkjet printing, we used them as electrodes in order to fabricate electrochromic cells of the following configuration: Glass/FTO/WO_3/electrolyte/Ce-modified TiO_2/FTO/Glass. Electrochromic cells with typical dimensions of 9 cm × 10 cm were prepared as follows: The anode FTO/Ce-modified TiO_2 and the cathode FTO/WO_3 were placed opposite to each other with their conductive sides slightly removed so as to maintain the appropriate space for electrical contacts. The space between the two electrodes was filled with the electrolyte. The liquid form of the electrolyte was inserted through a hole that was drilled into one of the two glasses, while the space was fixed in place to a distance of 50 micrometers by the application of thermoplastic material (DuPont Surlyn®) around the glass. After 30 min the electrolyte turns to a gel, due to the esterification reaction of the alkoxy groups at both edges of the hybrid material ED-600-ICS.

3. Results and Discussion

3.1. Microstructure Properties of Both Electrodes

3.1.1. WO_3 Films

The analysis of the structure and morphology of the WO_3 films were carried out using scanning electron microscopy (SEM). Figure 2a shows the SEM image of the surface of the WO_3 film printed on FTO coated glass. The film seems to be homogeneous over the entire surface area. Furthermore, it is obvious that particles formed with sizes in the range of 20–40 nm. It is also obvious from the image that WO_3 particles are not agglomerated in high grade, creating a porous structure within the film. Figure 2b illustrates the cross section image of the as-prepared film. It can be seen that the film was successfully deposited on the substrate and the thickness of the layer was between 390 to 400 nm. In addition, it is clear that the electrochromic layer is not compact in contrast to the FTO layer (647 nm) on the bottom, which facilitates the electrolytes' pouring into the pores of WO_3 film.
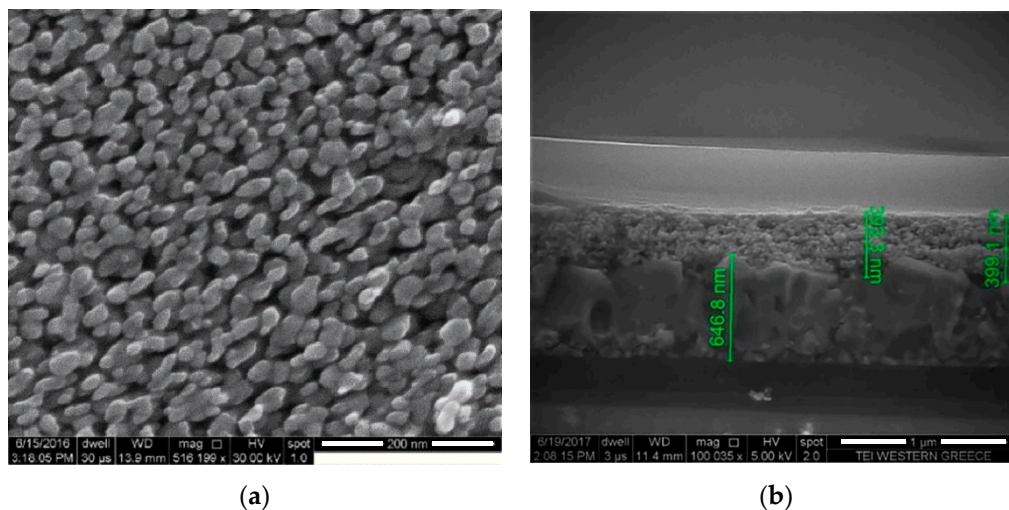
Figure 2. (**a**) Top view field-emission electron microscopy (FESEM) image and (**b**) cross section image of WO$_3$ films.

3.1.2. Ce-Modified TiO$_2$ Films

The morphology of the Ce-modified TiO$_2$ films employed as ion storage layers in EC devices is presented in Figure 3. Moreover, we also present pristine TiO$_2$ films for comparison with those modified with cerium. The films proved to be in both cases very homogenous while in the case of Ce-modified TiO$_2$ the particles were even smaller. This was verified by the TEM image shown in the same figure. The average size of TiO$_2$ particles was 10–12 nm (Figure 3a) while in the case of 10% Ce-TiO$_2$ the size was even smaller (7–8 nm) (Figure 3b). The decrease of particle size can be attributed to the specific interaction of Ce ions at the interface of titanium dioxide particles, which prevents TiO$_2$ anatase particles from adhering together and inhibits the growth of crystal grains [54]. We examined the XRD spectrum of the composite film containing Ce ions (10% w/w) where a new peak at about $2\theta = 30.8°$ (Figure S1) was also observed among the characteristic peaks of anatase [JCPDS ICDD card No. 21-1272]. It most probably means that a new crystal phase corresponding to cerium titanate Ce$_x$T$_{(1-x)}$O$_2$ was formed. The intensity of this peak increased along with the concentration of Ce ions in the starting sol. This peak cannot be attributed to common cerium oxides (CeO$_2$, Ce$_2$O$_3$, CeO, etc.). However, a more detailed examination of the spectrum may indicate the existence of brookite in XRD patterns, which is evidenced from the presence of the (211) peak at $2\theta = 30.68°$ (JCPDS ICDD cards No. 76-1937). However, the cerium atoms are undoubtedly present in the films and for that reason we prefer the term cerium modified TiO$_2$ films. As the particles' dimensions are very small in the case of Ce-modified TiO$_2$, a TEM image was selected to fully characterize and certify the accurate size in this case (Figure 3c). Our initial predictions were proved correct, as it was found that the size of the particles was around 8 nm. The thickness of the Ce-modified TiO$_2$ films was around 590 nm according to the cross section image of (Figure 3d).
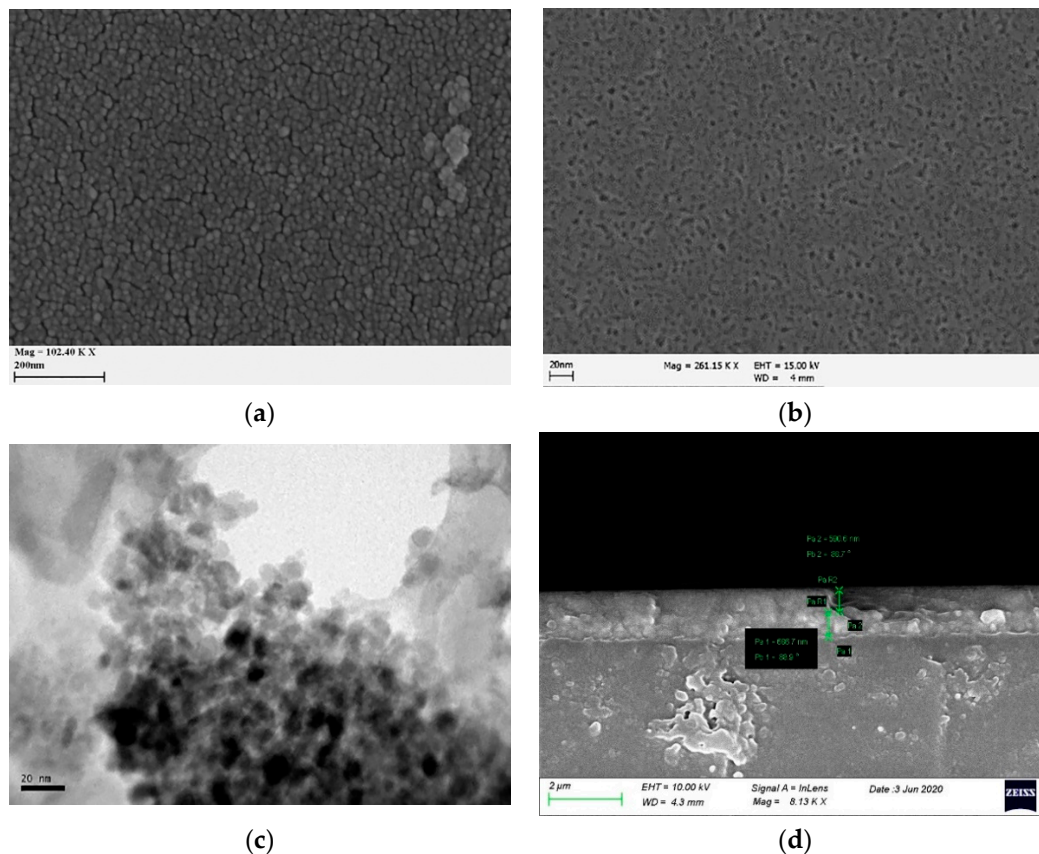
(a)

(b)

(c)

(d)

Figure 3. Top-view of (**a**) TiO_2, (**b**) Ce- modified TiO_2 film, (**c**) TEM image of particles scratched from a Ce- modified TiO_2 film and (**d**) cross section view of a Ce- modified TiO_2 film (from [55] with copyright permission from Elsevier).

3.2. BET Surface Areas for Ce-TiO_2 and Pristine TiO_2 Films

Porosity of the ion storage layer is very important to the operation of electrochromic devices, therefore we performed measurements to have an estimation of this parameter. Nitrogen sorption–desorption isotherms and the corresponding pore size distribution curve are shown in Figure 4. The isotherms for the samples of 10% Ce-TiO_2 and pristine TiO_2 used as a comparison show that the sorption starts at $P/P_0 \approx 0.5$–0.8; that is due to the capillary condensation in the mesoporous structure while the pore size distribution is narrow and centers at around 7 nm. The BET specific surface area (SSE) for Ce-modified samples is relatively high and was calculated at 151 m^2/g compared to 121 m^2/g for pristine TiO_2. The total pore volume (V_p) was measured at 0.220 cm^3/g for cerium modified TiO_2 films, while it was found to be 0.133 cm^3/g for pristine TiO_2 films. From data presented for both samples it is obvious that the presence of cerium leads to higher values for SSE, which is a promising result for the as-prepared cerium-modified TiO_2 films to be employed as ion storage films in electrochromic devices. The porosity of the films was also calculated to be 34% and 43% for pristine TiO_2 and cerium-modified TiO_2 samples, respectively.
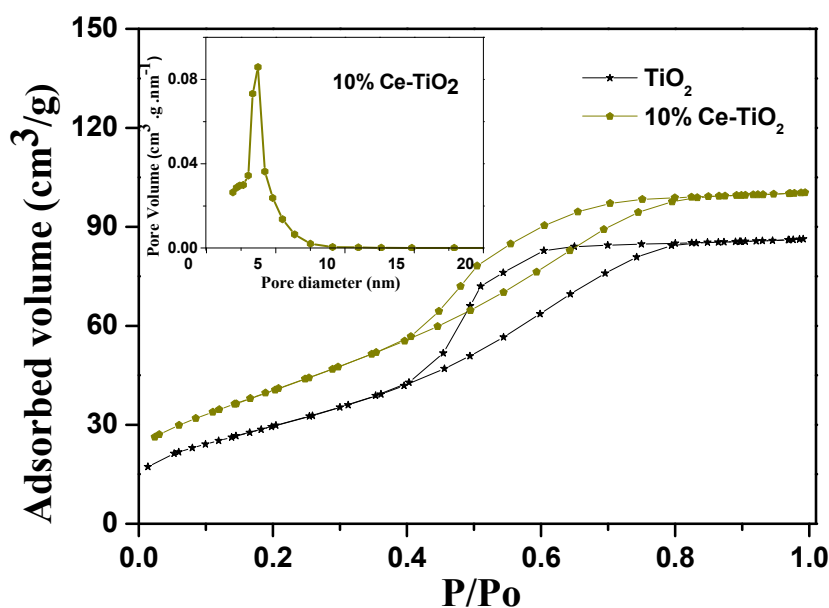
Figure 4. Sorption–desorption curves for pristine TiO$_2$ and cerium-modified TiO$_2$ films and pore size distribution (inset) of 10% cerium-modified TiO$_2$ films (adapted from [55] with copyright permission from Elsevier).

3.3. Electrochemical Characterization of Electrochromic and Ion Storage Film.

The electrochemical properties of electrochromic and ion storage films, developed in this work, were investigated using the cyclic voltammetry technique. Electrochemical measurements were carried out in a three-electrode cell with the use of an Autolab PGSTAT 302N electrochemical analyzer connected to a personal computer running NOVA software (Version 1.8, Metrohm AG, Herisau, Switzerland) in order to collect and analyze the experimental data. The working electrode was either the WO$_3$ film or the cerium-modified TiO$_2$ film deposited on FTO coated glass, the reference electrode was Ag/AgCl and the counter electrode was a platinum foil. A solution of 1M LiClO$_4$ in propylene carbonate served as the electrolyte. Cyclic voltammetry measurements for assessment of the WO$_3$ film were recorded with a linear potential sweep between −0.8V and +1.2V at various scan rates. It was observed that during the cathodic potential scan the film changed from colorless to deep blue, which indicated WO$_3$ reduction, followed by intercalation of lithium ions. On the other hand, during anodic potential scan the film turned transparent, which indicated WO$_3$ oxidation followed by de-intercalation of lithium ions.

An important parameter for the evaluation of electrochromic films is the diffusion coefficient (D). In order to calculate the diffusion coefficient of tungsten trioxide film, cyclic voltammograms at different scan rates namely: 30, 40, 50, 60, 80, 100, 120, and 150 mV/s were used as shown in Figure 5a. It is obvious that the shape of the curve is not altered with increasing scan rate. By using the current peak during anodic scans (i_{pa}), as it arises from cyclic voltammograms, the diffusion coefficient of the electrochromic film can be calculated, applying the Randles Sevcik Equation (3) [44,56]:

$$i_{pa} = 2.71 \times 10^5 \times n^{\frac{3}{2}} \times A \times C_o \times D^{\frac{1}{2}} \times v^{\frac{1}{2}} \tag{3}$$

where n is the number of electrons participating in the electrochemical reaction (n = 1 in redox pair W^{5+}/W^{6+}), A is the total surface area of the working electrode (in cm^2), C$_0$ is the concentration of active ions in the solution (in mol cm^{-3}) and ν is the scan rate (in V s^{-1}).
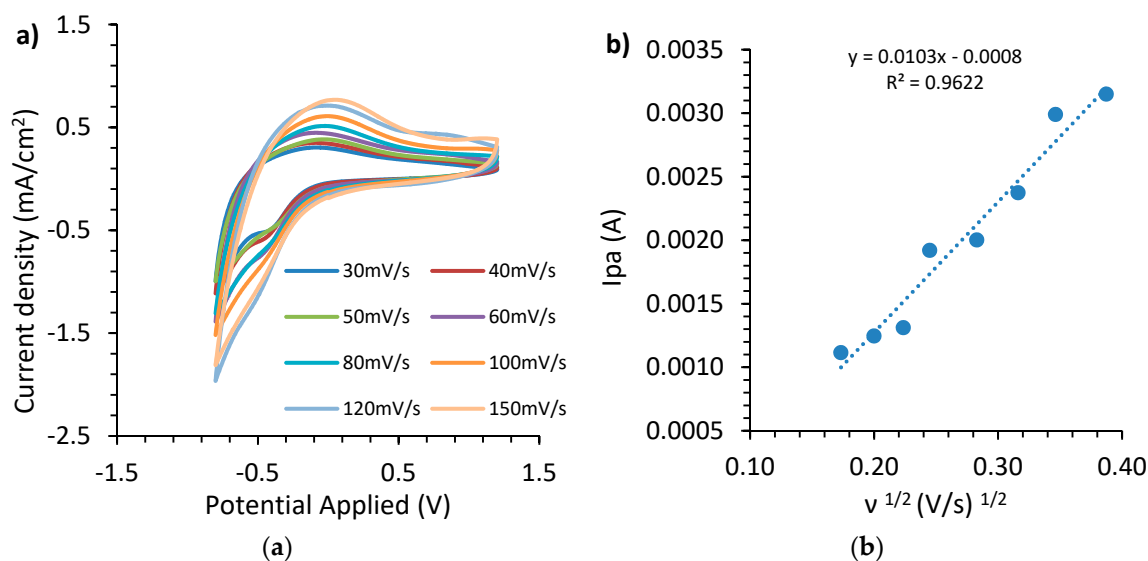
Figure 5. (**a**) WO_3 cyclic voltammetry curves at various scan rates, (**b**) plot of anodic peak current versus the square root of the scan rate.

Figure 5b indicates a linear relation between current anodic peaks during different scan rates with the square root of the scan rate, which confirms a controlled diffusion behavior. From the slope of the line in Figure 5b and after using Equation (3), the diffusion coefficient for WO_3 film was calculated to be 0.95×10^{-16} cm^2 s^{-1} for a film with active surface area of 3.89 cm^2 and 1 M concentration C_0 of lithium ions in the solution.

A similar procedure was followed in the case of a cerium-modified TiO_2 electrode for the evaluation of the diffusion coefficient (D); the results appear in Figure 6a.
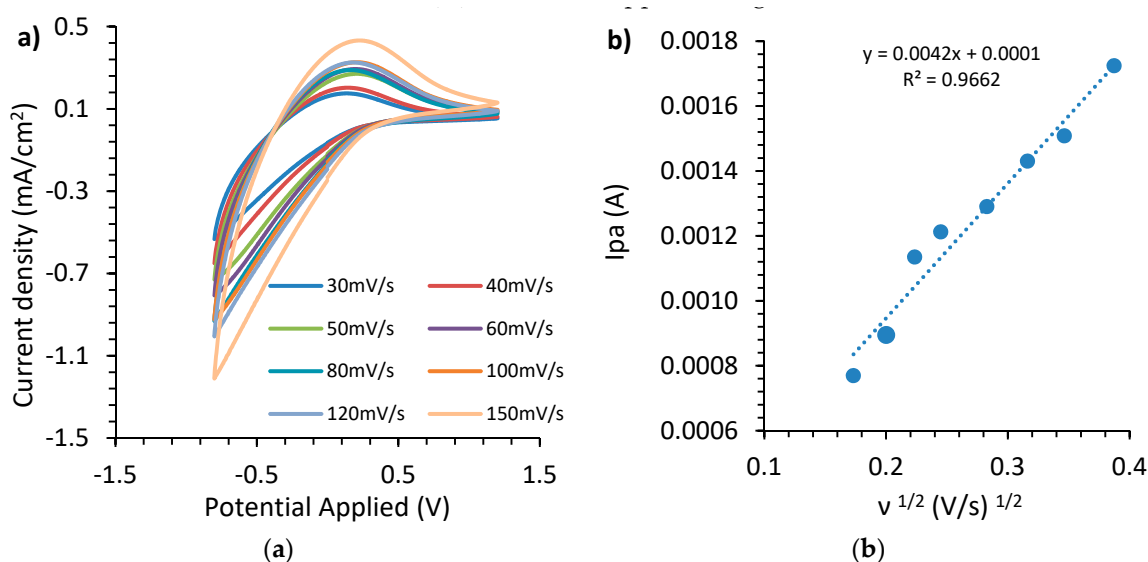

Figure 6. (**a**) Cerium-modified TiO_2 voltammetry curves at various scan rates, (**b**) plot of anodic peak current versus the square root of the scan rate.

Using again Equation (3) and calculating the slope of linear behavior between current anodic peaks during different scan rates with the square root of the scan rate, the diffusion coefficient for the cerium-modified TiO_2 electrode (Figure 6b) was calculated as 12.87×10^{-18} cm^2 s^{-1}.

Figure 7 shows the cyclic voltammograms for the Ce-modified TiO_2 film on FTO glass in comparison to TiO_2 on FTO glass and to plain FTO coated glass. The cyclic voltammetry measurements

were recorded at a scan rate of 10 mV/s between −1.0 V and 1.0 V. Charge capacity of inserted ions can be obtained from cyclic voltammetry data. Therefore, it was calculated using the following Equation [57]:

$$C = \int \frac{j \times dV}{s} \tag{4}$$

where j corresponds to the current density (mA cm^{-2}), V to the voltage applied (V), s to the scan rate (V s^{-1}) and C to the charge capacity (mC cm^{-2}).
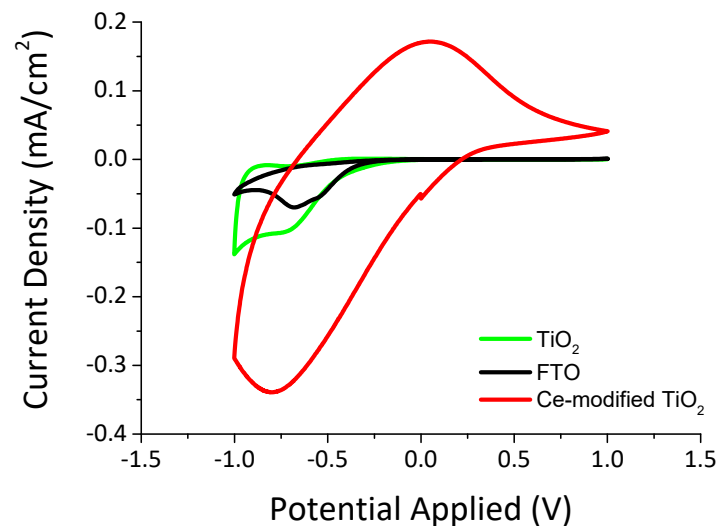

Figure 7. Cyclic voltammograms for SnO$_2$:F (FTO), TiO$_2$ and Ce-modified TiO$_2$ coated glasses measured at a scan rate 10 mV/s.

Table 1 shows the charge capacity of inserted ions calculated from Equation (4). It is obvious that the charge capacity of FTO coated glass (4.26 mC cm^{-2}) and of TiO$_2$ (6.21 mC cm^{-2}) is much smaller than the charge capacity calculated for Ce-modified TiO$_2$ film (26.77 mC cm^{-2}).

Table 1. Comparison of charge capacity of the measured films.

Counter Electrode	Charge Capacity (mC cm^{-2})
SnO$_2$:F (FTO)	4.26
TiO$_2$/FTO	6.21
Ce-modified TiO$_2$/FTO	26.77

In conclusion, Ce-modified TiO$_2$ film is appropriate to be used as an ion storage layer at electrochromic devices due to its high charge capacity.

3.4. Evaluation of Electrochromic Device

For the assessment of the electrochromic device with configuration of Glass/FTO/WO$_3$/Quasi-solid-state electrolyte/Ce-modified TiO$_2$/FTO/Glass chronoamperometry was used. Chronoamperometry measurements were recorded with the potential being stepped from 0 to +2.5 V for 10 min while performing the coloring procedure and from 0 to −0.3 V for 15 min while performing the bleaching procedure as shown in Figure 8. The fabricated device appeared dark blue in the colored state as depicted in Figure 9a and became transparent after the bleaching cycle as shown at Figure 9b.
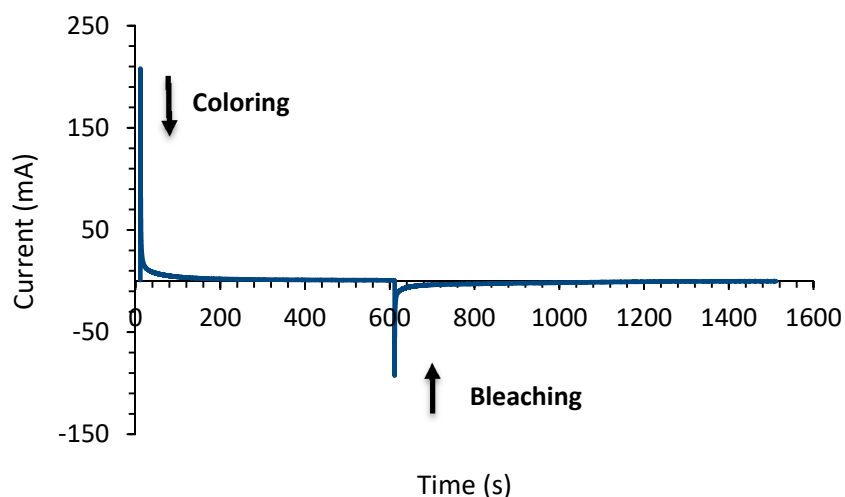
Figure 8. Chronoamperometry curve of the electrochromic cell appearing both at the bleached and the tinted states.
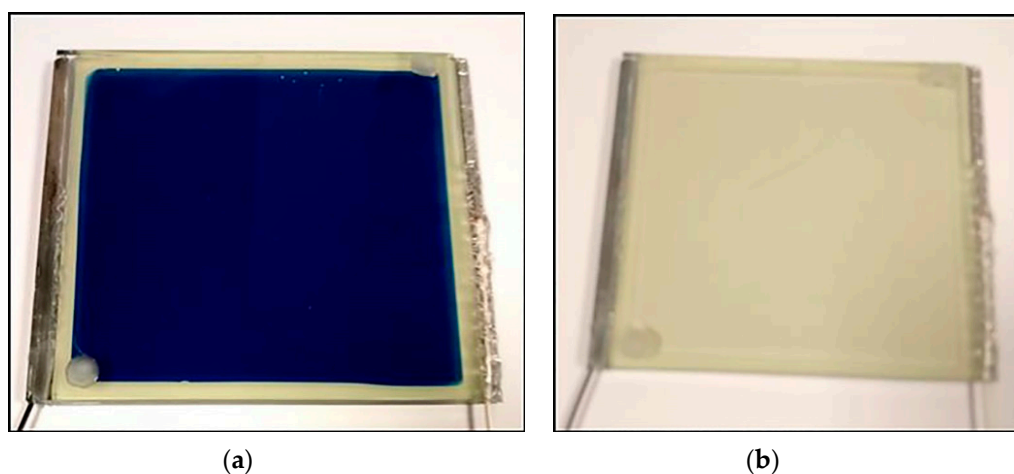

| (a) | (b) |

Figure 9. (**a**) Tinted and (**b**) bleached state of the fabricated electrochromic device with dimensions: 9 cm × 10 cm.

Furthermore, Figure 10 illustrates the corresponding transmittance spectra of the cell at the colored and the bleached states. As can be seen in the figure, the transmittance of the device in the colored state was measured to be 13.26% at 550 nm while at the bleached state it was 71.64% measured at the same wavelength. We conclude that there is an 81.5% reduction of transmittance because of the coloring procedure. Furthermore, we note the obvious reduction of the transmittance at both stages in the infrared region even at the bleached stage (cf. Figure S2). This means that present electrochromic devices, with the use of specific quasi-solid-state electrolyte, could contribute to the thermal relief of a building by substituting the normal glass panes with a specific electrochromic material, due to the obvious reduction of the infrared (thermal) radiation.
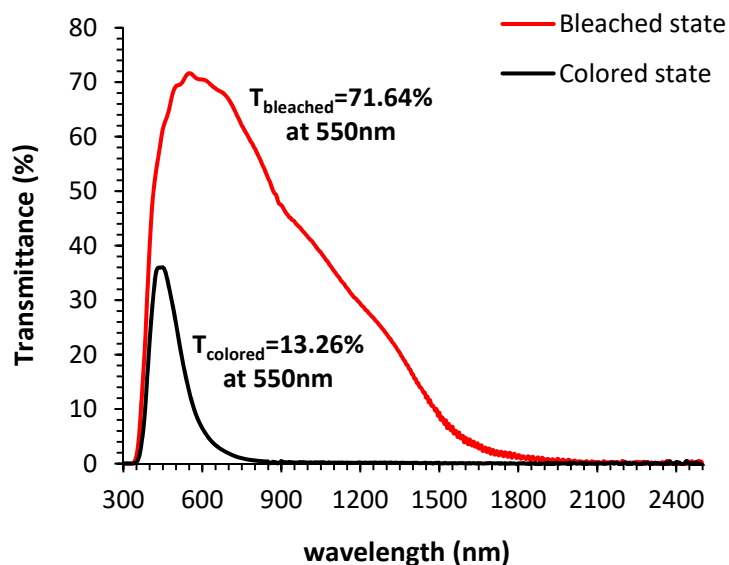
Figure 10. Transmittance of fabricated electrochromic cell at the colored state and the bleached state.

Figure 11 represents the variation of charge inserted to and extracted from the electrochromic device during the coloration and bleaching process respectively.
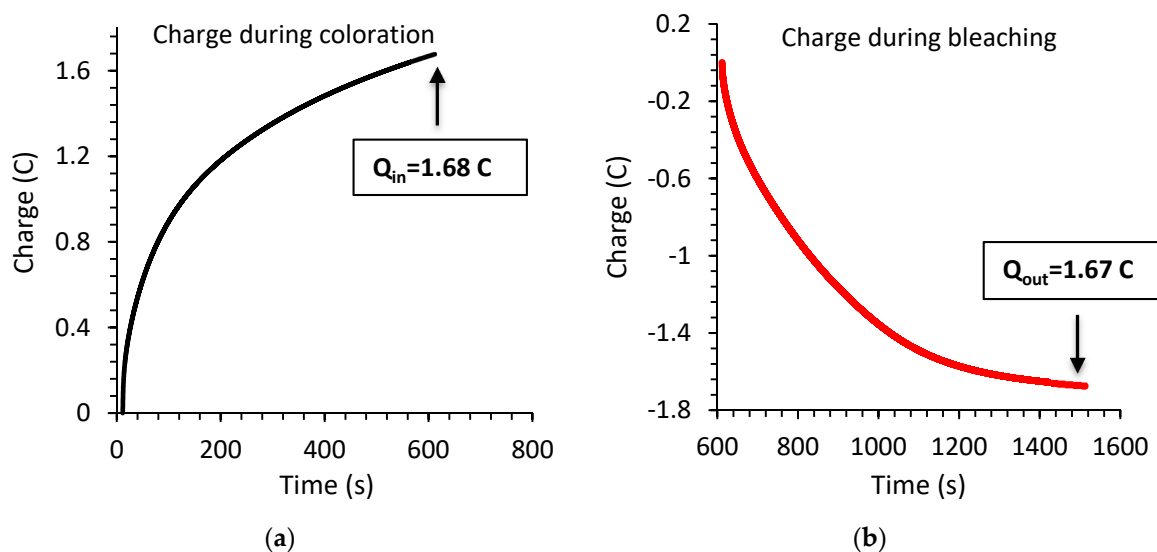

Figure 11. Variation of charge **(a)** inserted into the electrochromic device and **(b)** extracted from the electrochromic device.

As can be found the device shows an excellent reversibility as the charge inserted into the device (1.68 C) during coloration is equivalent to the charge extracted (1.67 C) from the device during bleaching. A very important parameter in order to evaluate an electrochromic device is coloration efficiency (CE). The CE at a particular wavelength, $\eta(\lambda)$, is calculated by the following Equation [58]:

$$\eta(\lambda) = \frac{\Delta OD(\lambda)}{Q_{in}} = \frac{\Delta OD(\lambda)}{\frac{q_{in}}{A}} \tag{5}$$

therein, Q_{in} is the intercalated charge per unit electrode area (C cm^{-2}), q_{in} is the intercalated charge (C) and A is the area of the electrode (cm^{-2}). Furthermore $\Delta OD(\lambda)$ is the change in optical density, a dimensionless quantity given as follows [58]:

$$\Delta OD(\lambda) = \log \frac{T_b(\lambda)}{T_c(\lambda)} \tag{6}$$

where $T_b(\lambda)$ and $T_c(\lambda)$ is the transmittance of the device in its bleached and tinted state at a particular wavelength (550nm), respectively. Based on Equation (6) the change in optical density was found to be $\Delta OD(\lambda) = 0.73$. Furthermore, from Equation (5) the coloration efficiency of the electrochromic device is $CE = 30.97$ cm^2/C for $q_{in} = 1.68$ C and $A = 71.28$ cm^2 as shown in Table 2.

Table 2. Electrochromic properties of the fabricated device.

EC Device	T_b (%) *	T_c (%) *	$\Delta OD(\lambda)$	q_{in} (C)	A (cm^2)	η (cm^2/C)
9 cm × 10 cm	71.64	13.26	0.73	1.68	71.28	30.97

* measured at 550 nm.

The long-term cycling stability of the electrochromic cell was also evaluated by observing the loss of optical contrast upon repetitive cycling. The device succeeded to keep more than 93% of its maximum optical contrast during the application of boundary potentials in the form of square-wave pulses for over one hundred and fifty successive cycles with no obvious malfunction (cf. Figure S3).

Finally, in terms of electrochemical energy storage performance, we calculated the energy density (E in Wh cm^{-2}), the energy power density (P in W m^{-2}) and the areal capacitance (C$_a$ in F cm^{-2}) of the electrochromic device prepared in this work. The aforementioned calculations were estimated with the use of the following Equations [59]:

$$E = \frac{E_t}{A} \tag{7}$$

$$P = \frac{E}{\Delta t} \tag{8}$$

$$C_a = \frac{C_{eff}}{A} \tag{9}$$

where E_t (Wh) is the amount of total energy that is released from the device during the discharging procedure, A is the area of the electrode (cm^2) and Δt is the discharging time (s). Furthermore, C_{eff} (F) is the effective capacitance, which is calculated as follows:

$$E_t = \frac{1}{2}C_{eff}V^2 \Leftrightarrow C_{eff} = \frac{2 \times E_t}{V^2} \tag{10}$$

where V is the voltage of the cell.

As shown in Table 3, the electrochromic device studied in this work has an energy density of 1.95×10^{-3} mWh cm^{-2} and a high areal capacitance of 156.2 mF cm^{-2}, so it could be a promising candidate for future applications into smart buildings.

Table 3. Calculation of energy density, energy power density and areal capacitance of the fabricated electrochromic device.

EC Device	E (mWh cm^{-2})	P (mW cm^{-2})	C$_a$ (mF cm^{-2})
9 cm × 10 cm	1.95×10^{-3}	7.82×10^{-3}	156.2

4. Conclusions

In the above experiments, we presented the good matching between WO_3 and Ce modified TiO_2 electrodes in electrochemical and electrochromic properties in large-scale devices using quasi-solid electrolyte. In particular, nanocrystalline WO_3 and Ce modified TiO_2 electrodes prepared via the sol-gel method exhibited porous structure consisting of 20–40 and 7–8 nm particle size, respectively. Especially for the counter electrode a very high particle specific area of 151 m^2/g was measured for Ce modified TiO_2, which is 25% higher than pristine TiO_2; additionally Ce modified TiO_2 is 26% more porous, which is very important for electrochromic applications. The charge capacity of the Ce-TiO_2 electrode was 26.77 mC/cm^2, much higher than 6.21 mC/cm^2 measured for TiO_2. The quasi-solid-state electrochromic device in dimensions 9 x 10 cm exhibited a wide optical contrast of 13 to 72% in a cell's transmittance measured at 550 nm in a low activation voltage window of +2.5 to −0.3 volts. The additional benefit of the energy storage by monitoring high areal capacitance (156.2 mF/cm^2) makes this electrode combination attractive to smart energy saving applications.

Supplementary Materials: The following are available online at http://www.mdpi.com/1996-1944/13/14/3241/s1, Figure S1: XRD of pristine TiO_2 and cerium modified films, Figure S2: Transmittance (%) vs wavelength for (a) plain glass, (b) FTO glass, (c) tungsten trioxide over FTO glass and (d) complete EC device, Figure S3: Transmittance(%) measured at 550nm vs number of cycles for the 9 cm × 10 cm device.

References

1. Granqvist, C.G. Chromogenic materials for transmittance control of large-area windows. *Crit. Rev. Solid State Mater. Sci.* **1990**, *16*, 291–308. [CrossRef]

2. Thummavichai, K.; Xia, Y.; Zhu, Y. Recent progress in chromogenic research of tungsten oxides towards energy-related applications. *Prog. Mater. Sci.* **2017**, *88*, 281–324. [CrossRef]

3. Granqvist, C.G.; Lansaker, P.C.; Mlyuka, N.R.; Granqvist, G.A.; Avendano, E. Progress in chromogenics: New results for electrochromic and thermochromic materials and devices. *Sol. Energ. Mater. Sol. Cells* **2009**, *93*, 2032–2039. [CrossRef]

4. Granqvist, C.G. *Handbook of Inorganic Electrochromic Materials*, 1st ed.; Elsevier: Amsterdam, The Netherlands, 1995.

5. Niklasson, G.A.; Granqvist, C.G. Electrochromics for smart windows: Thin films of tungsten oxide and nickel oxide, and devices based on these. *J. Mater. Chem.* **2007**, *17*, 127–156. [CrossRef]

6. Runnerstrom, E.L.; Llordes, A.; Lounis, S.D.; Milliron, D. Nanostructured electrochromic smart windows: Traditional materials and NIR-selective plasmonic nanocrystals. *Chem. Commun.* **2014**, *50*, 10555–10572. [CrossRef] [PubMed]

7. Granqvist, C.G. Oxide electrochromics: An introduction to devices and materials. *Sol. Energ. Mater. Sol. Cells.* **2012**, *99*, 1–13. [CrossRef]

8. Zhai, Y.L.; Li, Y.; Zhang, H.; Yu, D.B.; Zhu, Z.J.; Sun, J.Z.; Dong, S.H. Self-rechargeable-battery-driven device for simultaneous electrochromic windows, ROS biosensing, and energy storage. *ACS Appl. Mater. Interfaces* **2019**, *11*, 28072–28077. [CrossRef]

9. Zhao, Q.; Fang, Y.S.; Qiao, K.; Wei, W.; Yao, Y.J.; Gao, Y.F. Printing of WO_3/ITO nanocomposite electrochromic smart windows. *Sol. Energy Mater. Sol. Cells.* **2019**, *194*, 95–102. [CrossRef]

10. Qu, H.; Zhang, H.; Zhang, X.; Zhang, X.; Tian, Y.; Wang, B.; Li, X.; Zhao, J.; Li, Y. Review: Recent progress in ordered macroporous electrochromic materials. *J. Mater. Sci.* **2017**, *52*, 11251–11268. [CrossRef]

11. Wang, B.; Man, W.; Yu, H.; Li, Y.; Zheng, F. Fabrication of Mo-Doped WO_3 nanorod arrays on FTO substrate with enhanced electrochromic properties. *Materials* **2018**, *11*, 1627. [CrossRef]

12. Dokouzis, A.; Theodosiou, K.; Leftheriotis, G. Assessment of the long-term performance of partly covered photoelectrochromic devices under insolation and in storage. *Sol. Energy Mater. Sol. Cells.* **2018**, *182*, 281–293. [CrossRef]

13. Bi, Z.; Li, X.; He, X.; Chen, Y.; Xu, X.; Gao, X. Integrated electrochromism and energy storage applications based on tungsten trioxide monohydrate nanosheets by novel one-step low temperature synthesis. *Sol. Energy Mater. Sol. Cells* **2018**, *183*, 59–65. [CrossRef]

14. Gillaspie, D.T.; Tenent, R.C.; Dillon, A.C. Metal-oxide films for electrochromic applications: Present technology and future directions. *J. Mater. Chem.* **2010**, *20*, 9585–9592. [CrossRef]

15. Xie, X.; Gao, C.; Du, X.; Zhu, G.; Xie, W.; Liu, P.; Tang, Z. Improved optical and electrochromic properties of NiO_x films by low-temperature spin-coating method based on NiO_x nanoparticles. *Materials* **2018**, *11*, 760. [CrossRef] [PubMed]

16. Zhu, Y.; Xie, L.; Chang, T.; Bell, J.; Huang, A.; Jin, P.; Bao, S. High performance all-solid-state electrochromic device based on Li_xNiO_y layer with gradient Li distribution. *Electrochim. Acta* **2019**, *317*, 10–16. [CrossRef]

17. Yano, J.; Noguchi, K.; Yamasaki, S.; Yamazaki, S. Novel color change of electrochromic iridium oxide in a matrix aramid resin film. *Electrochem. Commun.* **2004**, *6*, 110–114. [CrossRef]

18. Wu, C.-G.; Chung, M.-H. Water-soluble poly(2-(3thienyloxy)ethanesulfonic acid)/V_2O_5 nanocomposites: Synthesis and electrochromic properties. *J. Solid State Chem.* **2004**, *177*, 2285–2294. [CrossRef]

19. Lahav, M.; van der Boom, M.E. Polypyridyl metallo-organic assemblies for electrochromic applications. *Adv. Mater.* **2018**, 1706641. [CrossRef]

20. Beaujuge, P.M.; Reynolds, J.R. Color control in π-conjugated organic polymers for use in electrochromic devices. *Chem. Rev.* **2010**, *110*, 268–320. [CrossRef]

21. Banasz, R.; Wałęsa-Chorab, M. Polymeric complexes of transition metal ions as electrochromic materials: Synthesis and properties. *Coord. Chem. Rev.* **2019**, *389*, 1–18. [CrossRef]

22. Camino, D.; Deroo, D.; Salardenne, J.; Treuil, N. Counter electrode materials for lithium electrochromic devices. *Sol. Energ. Mater. Sol. Cells* **1995**, *39*, 349–366. [CrossRef]

23. Bhosale, A.K.; Tarwal, N.L.; Shinde, P.S.; Kadam, P.M.; Patil, R.S.; Barman, S.R.; Patil, P.S. Effective utilization of spray pyrolyzed CeO_2 as optically passive counter electrode for enhancing optical modulation of WO_3. *Solid State Ion.* **2009**, *180*, 1324–1331. [CrossRef]

24. Bhosale, A.K.; Shinde, P.S.; Tarwal, N.L.; Pawar, R.C.; Kadam, P.M.; Patil, P.S. Synthesis and characterization of highly stable optically passive $CeO_2–ZrO_2$ counter electrode. *Electrochim. Acta* **2010**, *55*, 1900–1906. [CrossRef]

25. Chen, H.S.; Jan, D.-J.; Lin, J.-H.; Wang, M.-C. Electrochromic, optical and binding-energy performances of tantalum pentoxide and zirconium dioxide films deposited with RF magnetron sputtering and cathodic arc plasma. *Sol. Energy Mater. Sol. Cells* **2019**, *203*, 110158. [CrossRef]

26. Wang, K.; Wu, H.; Meng, Y.; Zhang, Y.; Wei, Z. Integrated energy storage and electrochromic function in one flexible device: An energy storage smart window. *Energy Environ. Sci.* **2012**, *5*, 8384–8389. [CrossRef]

27. Wałęsa-Chorab, M.; Skene, W.G. Investigation of an electroactive immobilized azomethine for potential electrochromic use. *Sol. Energy Mater. Sol. Cells* **2019**, *200*, 109977.

28. Jensen, J.; Hösel, M.; Dyer, A.L.; Krebs, F.C. Development and manufacture of polymer-based electrochromic devices. *Adv. Funct. Mater.* **2015**, *25*, 2073–2090. [CrossRef]

29. Kamal, H.; Elmaghraby, E.K.; Ali, S.A.; Abdel-Hady, K. The electrochromic behavior of nickel oxide films sprayed at different preparative conditions. *Thin Solid Films* **2005**, *483*, 330–339. [CrossRef]

30. Tenent, R.C.; Gillaspie, D.T.; Miedaner, A.; Parilla, P.A.; Curtis, C.J.; Dillon, A.C. Fast switching electrochromic Li^+-doped NiO Films by ultrasonic spray deposition. *J. Electrochem. Soc.* **2010**, *157*, H318–H322. [CrossRef]

31. Costa, C.; Pinheiro, C.; Henriques, I.; Laia, C.A.T. Inkjet printing of sol-gel synthesized hydrated tungsten oxide nanoparticles for flexible electrochromic devices. *ACS Appl. Mater. Interfaces* **2012**, *4*, 1330–1340. [CrossRef]

32. Livage, J.; Ganguli, D. Sol-gel electrochromic coatings and devices: A review. *Sol. Energy Mater. Sol. Cells* **2001**, *68*, 365–381. [CrossRef]

33. Baeck, S.-H.; Choi, K.-S.; Jaramillo, T.F.; Stucky, G.D.; McFarland, E.W. Enhancement of photocatalytic and electrochromic properties of electrochemically fabricated mesoporous WO_3 thin films. *Adv. Mater.* **2003**, *15*, 1269–1273. [CrossRef]

34. Cai, G.; Cui, M.; Kumar, V.; Darmawan, P.; Wang, J.; Wang, X.; Lee-Sie Eh, A.; Qian, K.; Lee, P.S. Ultra-large optical modulation of electrochromic porous WO_3 film and the local monitoring of redox activity. *Chem. Sci.* **2016**, *7*, 1373–1382. [CrossRef] [PubMed]

35. Vidmar, T.; Topič, M.; Dzik, P.; Krašovec, U.O. Inkjet printing of sol–gel derived tungsten oxide inks. *Sol. Energy Mater. Sol. Cells* **2014**, *125*, 87–95. [CrossRef]

36. Mosiadz, M.; Tomov, R.I.; Hopkins, S.C.; Martin, G.; Hardeman, D.; Holzapfel, B.; Glowacki, B.A. Inkjet printing of $Ce_{0.8}Gd_{0.2}O_2$ thin films on Ni–5% W flexible substrates. *J. Sol–Gel Sci. Technol.* **2010**, *54*, 154–164. [CrossRef]

37. Cai, G.; Darmawan, P.; Cui, M.; Chen, J.; Wang, X.; Lee-Sie Eh, A.; Magdassi, S.; Lee, P.S. Inkjet-printed all solid-state electrochromic devices based on NiO/WO_3 nanoparticle complementary electrodes. *Nanoscale* **2016**, *8*, 348–357. [CrossRef]

38. Wojcik, P.J.; Cruz, A.S.; Santos, L.; Pereira, L.; Martins, R.; Fortunato, E. Microstructure control of dual-phase inkjet-printed a-WO_3/TiO_2/WO_X films for high-performance electrochromic applications. *J. Mater. Chem.* **2012**, *22*, 13268–13278. [CrossRef]

39. Cai, G.; Darmawan, P.; Cheng, X.; Layani, M.; Wei Ming Tan, A.; Li, S.; Lee-Sie Eh, A.; Gao, D.; Magdassi, S.; Lee, P.S. Direct inkjet-patterning of energy efficient flexible electrochromics. *Nano Energy* **2018**, *49*, 147–154. [CrossRef]

40. Kim, D.; Jeong, Y.; Koo, C.Y.; Song, K.; Moo, J. Thin film transistors with ink-jet printed amorphous oxide semiconductors. *Jpn. J. Appl. Phys.* **2010**, *49*, 05EB06-1–05EB06-4. [CrossRef]

41. Zhang, L.; Chao, D.; Yang, P.; Webber, L.; Li, J.; Kraus, T.; Fan, H.J. Flexible pseudocapacitive electrochromics via inkjet printing of additive-free tungsten oxide nanocrystal ink. *Adv. Energy Mater.* **2020**, *5*, 2000142. [CrossRef]

42. Zoski, C.G. *Handbook of Electrochemistry*, 1st ed.; Elsevier: Amsterdam, The Netherlands, 2007.

43. Bard, A.J.; Faulkner, L.R. *Electrochemical Methods: Fundamentals and Applications*, 2nd ed.; Wiley: New York, NY, USA, 2001.

44. Jovanovski, V.; Stathatos, E.; Orel, B.; Lianos, P. Dye-sensitized solar cells with electrolyte based on a trimethoxysilane-derivatized ionic liquid. *Thin Solid Film.* **2006**, *511–512*, 634–637. [CrossRef]

45. Stephan, A.M. Review on gel polymer electrolytes for lithium batteries. *Eur. Polym. J.* **2006**, *42*, 21–42. [CrossRef]

46. Kil, E.-H.; Choi, K.-H.; Ha, H.-J.; Xu, S.; Rogers, J.A.; Kim, M.R.; Lee, Y.-G.; Kim, K.M.; Cho, K.Y.; Lee, S.-Y. Imprintable, bendable, and shape-conformable polymer electrolytes for versatile-shaped lithium-ion batteries. *Adv. Mater.* **2013**, *25*, 1395–1400. [CrossRef] [PubMed]

47. Dong, R.-X.; Shen, S.-Y.; Chen, H.-W.; Wang, C.-C.; Shih, P.-T.; Liu, C.-T.; Vittal, R.; Lin, J.-J.; Ho, K.-C. A novel polymer gel electrolyte for highly efficient dye-sensitized solar cells. *J. Mater. Chem. A* **2013**, *1*, 8471–8478. [CrossRef]

48. Yang, X.; Zhang, F.; Zhang, L.; Zhang, T.; Huang, Y.; Chen, Y. A High-performance graphene oxide-doped ion gel as gel polymer electrolyte for all-solid-state supercapacitor applications. *Adv. Funct. Mater.* **2013**, *23*, 3353–3360. [CrossRef]

49. Kang, Y.J.; Chun, S.-J.; Lee, S.-S.; Kim, B.-Y.; Kim, J.H.; Chung, H.; Lee, S.-Y.; Kim, W. All-solid-state flexible supercapacitors fabricated with bacterial nanocellulose papers, carbon nanotubes, and triblock-copolymer ion gels. *ACS Nano* **2012**, *6*, 6400–6406. [CrossRef]

50. Sygkridou, D.; Rapsomanikis, A.; Stathatos, E. Functional transparent quasi-solid state dye-sensitized solar cells made with different oligomer organic/inorganic hybrid electrolytes. *Sol. Energy Mater. Sol. Cells* **2017**, *159*, 600–607. [CrossRef]

51. Stathatos, E. Organic-inorganic nanocomposite materials prepared by the sol-gel route as new ionic conductors in quasi solid state electrolytes. *Ionics* **2005**, *11*, 140–145. [CrossRef]

52. Stathatos, E.; Lianos, P.; Del Monte, F.; Levy, D.; Tsiourvas, D. Formation of TiO_2 nanoparticles in reverse micelles and their deposition as thin films on glass substrates. *Langmuir* **1997**, *13*, 4295–4300. [CrossRef]

53. Choi, H.; Stathatos, E.; Dionysiou, D.D. Synthesis of nanocrystalline photocatalytic TiO_2 thin films and particles using sol–gel method modified with nonionic surfactants. *Thin Solid Film.* **2006**, *510*, 107–114. [CrossRef]

54. Stengl, V.; Bakardijieva, S.; Murafa, N. Preparation and photocatalytic activity of rare earth doped TiO_2 nanoparticles. *Mater. Chem. Phys.* **2009**, *114*, 217–226. [CrossRef]

55. Rapsomanikis, A.; Apostolopoulou, A.; Stathatos, E.; Lianos, P. Cerium-modified TiO_2 nanocrystalline films for visible light photocatalytic activity. *J. Photochem. Photobiol. A* **2014**, *280*, 46–53. [CrossRef]

56. Cai, G.-F.; Wang, X.-L.; Zhou, D.; Zhang, J.-H.; Xiong, Q.-Q.; Gu, C.; Tu, J.-P. Hierarchical structure Ti-doped WO_3 film with improved electrochromism in visible-infrared region. *RSC Adv.* **2019**, *3*, 6896–6905. [CrossRef]

57. Wen, R.-T.; Granqvist, C.G.; Niklasson, G.A. Eliminating degradation and uncovering ion-trapping dynamics in electrochromic WO_3 thin films. *Nature Mater.* **2015**, *15*, 991–1001. [CrossRef]

58. Au, B.W.-C.; Chan, K.Y.; Knipp, D. Effect of film thickness on electrochromic performance of sol-gel deposited tungsten oxide (WO_3). *Opt. Mater.* **2019**, *94*, 387–392.

59. Zhong, Y.; Chai, Z.; Liang, Z.; Sun, P.; Xie, W.; Zhao, C.; Mai, W. Electrochromic asymmetric supercapacitor windows enable direct determination of energy status by naked eye. *ACS Appl. Mater. Interfaces* **2017**, *9*, 34085–34092. [CrossRef]